Available online at www.CivileJournal.org

Civil Engineering Journal

(E-ISSN: 2476-3055; ISSN: 2676-6957)

Vol. 10, No. 11, November, 2024

An Investigation of Dynamic Soil-Structure Interaction on the Seismic Behavior of RC Base-Isolated Buildings

Alvin K. Santoso [1], Taiki Saito [1*]

[1] *Department of Architecture and Civil Engineering, Toyohashi University of Technology, Toyohashi, Aichi, 441-8580, Japan.*

Received 10 August 2024; Revised 12 October 2024; Accepted 19 October 2024; Published 01 November 2024

Abstract

Soil-structure interaction (SSI) can significantly influence earthquake responses in base-isolated (BI) buildings, yet it is often overlooked in practice due to the high computational demands of complex analyses. This study investigates SSI effects on reinforced concrete (RC) base-isolated buildings, idealizing SSI with a cone model. Three BI building models of varying heights and soil characteristics were analyzed using modal and nonlinear time history analysis. The base isolation system incorporated elastic sliding bearings, lead rubber bearings, natural rubber bearings, and oil dampers. The SSI model was idealized considering hard, medium, and soft soils. To simulate earthquake input, three artificial ground motions with different phase characteristics were generated to match the design response spectrum according to the Japanese code. The seismic responses of the base-isolated building models with SSI were compared to those of models without SSI. Modal analysis showed that the natural period increased with softer soil profiles. In the first and second modes, the natural period lengthened as the building's aspect ratio increased. Conversely, in the higher modes with a rocking pattern, the building with the lowest aspect ratio exhibited the longest natural period. Overall, implementing SSI generally reduced seismic responses, notably lowering story drift, acceleration, and force, particularly for buildings on soft soil. However, the SSI effect significantly increased the base rotation angle in high aspect ratio buildings on soft and medium soils. These findings indicate that including SSI in analysis is essential for more realistic seismic response predictions, especially for tall, slender base-isolated buildings.

Keywords: Base Isolated Building; Soil-Structure Interaction; Cone Model; Nonlinear Time History Analysis; Modal Analysis.

1. Introduction

Numerous earthquakes have caused significant damage to buildings, underscoring the need for disaster prevention measures to enhance building safety. One effective approach is improving building performance through base isolation techniques, which involve separating the superstructure from the foundation by installing low-stiffness devices that decouple the building from the horizontal component of ground motion [1]. This increases the building's natural period, thereby reducing the force transmitted from the ground to the superstructure. Several studies have evaluated the effectiveness of base isolation in enhancing building performance. Ziraoui et al. [2] assessed the use of lead rubber bearings (LRBs) to improve the seismic resilience of reinforced concrete buildings through numerical analysis. Their findings indicated that story displacement and inter-story drift, base shear, and moments were reduced by 50%, 60%, and 70%, respectively, compared to non-isolated buildings. Similarly, Usta [3] conducted a finite element simulation to examine the seismic performance of a historical masonry mosque using nonlinear time history analysis, showing that LRBs increased the building's natural period while reducing displacement, acceleration, and forces on the structure. These findings suggest that base isolation systems are an effective method for protecting structures from severe earthquake damage.

* Corresponding author: saito.taiki.bv@tut.jp

http://dx.doi.org/10.28991/CEJ-2024-010-11-01

Conventional seismic analyses assume that base-isolated buildings rest on rigid soil, thereby ignoring soil-structure interaction (SSI). However, different soil characteristics introduce varying levels of flexibility into the system, which, in combination with base isolation, can impact the overall building response. This flexibility is influenced by factors such as shear wave velocity and soil layer depth [4]. Alavi & Alidoost [5] and Hatami et al. [6] examined SSI effects on base-isolated and non-isolated buildings of different heights, represented by aspect ratios (the ratio of building height to the equivalent foundation radius) ranging from 0.8 to 4.0. Their results indicated that the natural period of base-isolated buildings with high aspect ratios on soft soil increased by up to 26%, whereas SSI effects on the natural period were negligible in stiffer soil conditions. Additionally, for base-isolated buildings with high aspect ratios, the base shear and relative displacement decreased by 10% to 28%, while base rocking might increase due to the effects of soft soil. A parametric study by Du et al. [7] used a 2-degree-of-freedom model with sway and rocking springs in dynamic analysis to examine base-isolated buildings in the frequency domain. Their findings highlighted that SSI effects are more pronounced in tall, slender base-isolated buildings than in low-rise structures. Furthermore, nonlinear time history analysis of base-isolated shear-frame structures with a mass-spring dashpot model revealed that base shear, story acceleration, story displacement, and the overall effectiveness of the base isolation system decreased with increasing soil flexibility [8]. Forcellini [9] conducted finite element analysis showing that SSI can reduce base shear while increasing the natural period and base displacement of base-isolated buildings. Additionally, Cruz & Miranda [10] evaluated SSI effects on the equivalent damping ratio in non-isolated buildings, finding that the damping ratio decreased in tall, slender buildings but increased in low, squat buildings with SSI.

Various methods have been developed to model soil-structure interaction (SSI), including the single degree of freedom mass-spring dashpot [11, 12], elastic half-space [13, 14], continuum approaches, finite element method [15], and the cone model [16-18]. The mass-spring-dashpot model represents the foundation as a single mass connected to a linear spring and damper, capturing the soil's stiffness and damping. However, this model is limited in that it cannot account for frequency-dependent effects or additional damping coefficients that may influence dynamic SSI [19]. In the elastic half-space model, the foundation is idealized as a cylindrical disk on a homogeneous elastic half-space, with a uniformly distributed vertical load beneath the footing. However, actual soil conditions rarely exhibit homogeneity, as layered soil and rigid rock layers are often present, which can increase resonance frequency [20, 21]. The continuum method simplifies the rigid foundation as a lumped parameter model on elastic half-space soil, applying an impedance function to account for displacement under vertical load, thus incorporating soil stiffness and damping. The finite element method idealizes soil as three-dimensional, axisymmetric solid elements or two-dimensional plane strain elements. Although this approach is highly accurate, it demands significant computational resources [15].

The cone model represents a massless, rigid foundation on the surface of a homogeneous half-space, modeled using truncated semi-infinite elements that account for wave propagation effects through complex stiffness and wave mechanics principles [16-18]. The truncated area expands with increasing depth, resembling a cone. This approach simplifies the complex behavior of soil by replacing it with sway and rocking springs, as well as dampers, to simulate soil and foundation radiation damping. Compared to simpler models like the mass-spring-dashpot, the cone model better accounts for higher damping effects, offering greater accuracy under dynamic loading conditions [19]. Additionally, the cone model represents an elastic half-space by limiting the propagated area to the soil region that significantly influences the foundation's response, disregarding areas outside the cone with minimal structural impact. This model is valid for both low and high frequencies, accurately capturing the static stiffness and radiation damping characteristics of an elastic half-space [22]. However, this method does not account for the plastic deformation in soil, residual displacements, or foundation-soil separation, as it assumes an elastic soil behavior. Therefore, for complex and critical structures, more advanced methods, such as continuum and finite element modeling, may be necessary. Although these methods offer greater accuracy, they require complex modeling and come with high computational costs.

Several studies have examined SSI effects on the dynamic response of structures using the cone model approach. For example, Bararnia et al. [23] investigated the combined effects of SSI and nonlinear superstructure behavior on the inelastic displacement ratios of soil-structure systems with embedded foundations, focusing on kinematic interaction and rocking foundation input motion. Hassani et al. [24] evaluated inelastic displacement ratios for degraded structures considering SSI, with a focus on different hysteresis models and the impact of SSI on nonlinear responses, particularly for strength-stiffness degrading systems. Lu et al. [25] enhanced the accuracy of the replacement oscillator approach for SSI analysis of flexible-based structures on soft soil, while Ganjavi et al. [26] investigated SSI impacts and lateral load patterns on the seismic response of steel moment-resisting frames designed with performance-based plastic design, proposing new ductility-dependent strength reduction factors for flexible base conditions. However, the effects of SSI on base-isolated buildings using the cone model have not been addressed in prior studies.

This study investigates the seismic behavior of reinforced concrete (RC) base-isolated buildings through nonlinear time history (NLTH) and modal analysis. The cone model is employed to idealize soil-structure interaction (SSI) due to its simplicity, efficiency, and low computational cost, while still effectively representing soil dynamic wave propagation. Three building models (5, 10, and 15 stories) were designed according to Japanese design provisions and analyzed in STERA 3D v11.5 [27]. The seismic responses, including inter-story drift, displacement, acceleration, base shear, and base rotation, were compared by incorporating SSI effects across different soil types (hard, medium, and soft) and by evaluating base-isolated building models without SSI effects. The findings aim to emphasize the significance of SSI modeling and encourage practicing engineers to enhance base-isolated building analysis methods by considering SSI.

Section 2 details the research methodology, including the study workflow, preliminary design of the base-isolated building model, SSI idealization using the cone model, generation of spectrum-matched ground motions, and modeling method in STERA 3D v11.5. Section 3 presents the results and discussion, covering natural period, story displacement and drift, story acceleration, story shear, and base rotation. The study's conclusions are summarized in Section 4.

2. Methods

2.1. Workflow of the Study

The workflow of this study is illustrated in Figure 1. Three base-isolated building models (5, 10, and 15 stories) were designed to meet level 2 earthquake safety limits in accordance with the Japanese code, as outlined in reports by Ishiyama [28], Japan Society of Seismic Isolation (JSSI) [29], and in the study by Pietra et al. [30]. Three soil conditions were selected: hard (H), medium (M), and soft (S). Models without SSI are labeled as BI-H, BI-M, and BI-S, while models with SSI are labeled as SSI-H, SSI-M, and SSI-S, respectively. The cone model was used to calculate sway and rocking springs for the SSI-BI models, based on Caltrans' soil profile types as described by Wair et al. [31]. Additionally, three artificial ground motions were generated to align with the design response spectrum, following Japanese code provisions. Nonlinear time history (NLTH) and modal analysis were conducted to investigate the seismic behavior of all base-isolated (BI) models. The analysis results, including inter-story drift and displacement, story acceleration, story forces, base shear, and base rocking, were discussed and compared.

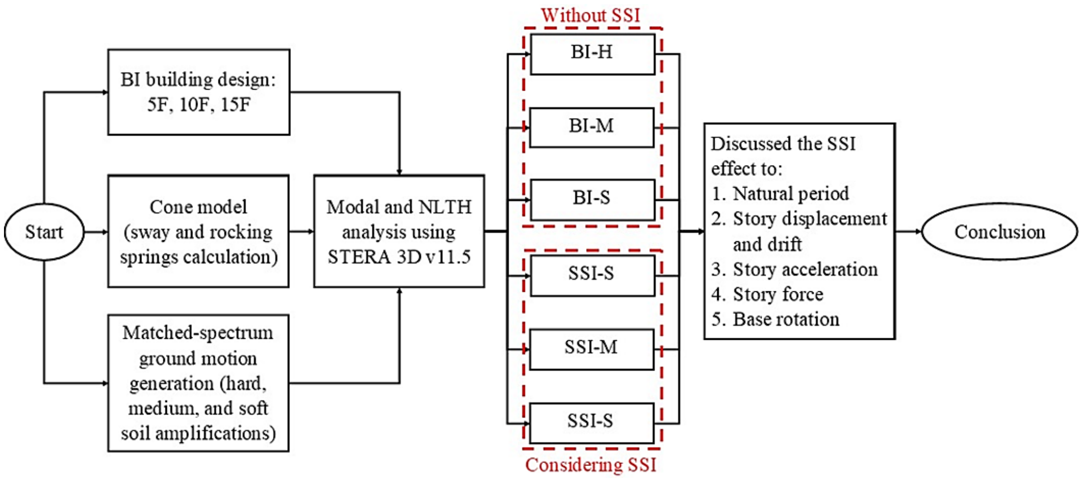

Figure 1. The study workflow

2.2. Preliminary Design of Base-Isolated Building

Three office buildings, with 5, 10, and 15 stories respectively, were designed using a reinforced concrete structure. Each story has a typical weight of 12 kN/m^2, while the weight of the story above the isolation layer was assumed to be 18 kN/m^2, 24 kN/m^2, and 30 kN/m^2 for the 5-, 10-, and 15-story cases, respectively. The height of each story in the superstructure is 4 m, and the isolation layer, designed for the repair and replacement of base isolation devices, has a height of 1.5 m. The elevation and plan views of all buildings are shown in Figure 2. An equivalent lateral force (ELF) method was initially applied to the non-isolated building system with fixed base supports to determine the adequate seismic capacity for each structural element. Base shear was calculated by multiplying the base shear coefficient by the total weight of the structure. As outlined in Ishiyama [28], the base shear coefficient (C_s) for the initial building design can be approximated using $C_s = 0.18/T$, where T represents the natural period of the non-isolated building. The natural period, T, was calculated using the formula $T = 0.02H$, where H is the total story height. The final base shear coefficient and natural period obtained from manual calculations and STERA 3D v11.5 are summarized in Table 1. The beam and column configurations were designed to be consistent every 5 stories, and the section properties of each building are detailed in Tables 2 and 3. Additionally, the material properties of the steel reinforcements were specified according to the Japanese Industrial Standard (JIS) [32].

Table 1. Base shear coefficient and natural period of the final building design results

Building	Base Shear Coefficient, *Cs*		Natural Period, *T* (sec)	
	Manual	STERA 3D	Manual	STERA 3D
5F	0.45	0.49	0.40	0.54
10F	0.23	0.33	0.80	0.86
15F	0.15	0.21	1.20	1.12

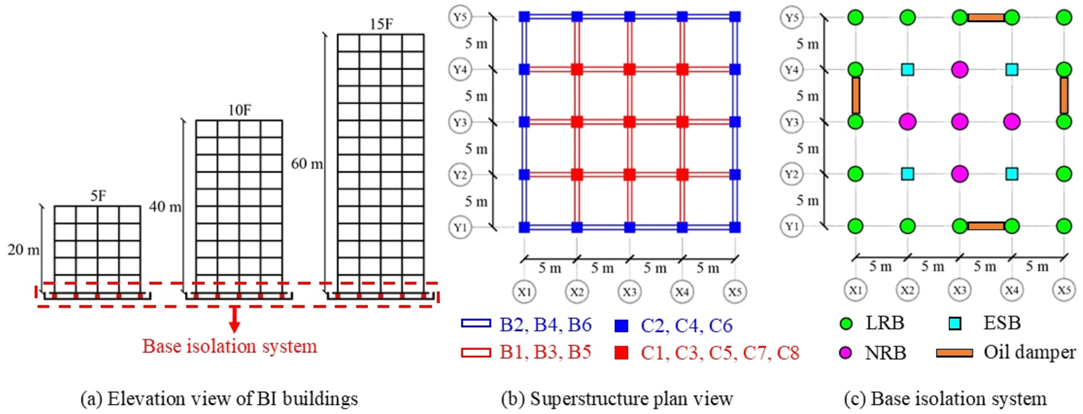

Figure 2. Elevation and plan views of the base-isolated building

Table 2. Beam section and material properties

No.	Building	Location	Section	Slab Thickness	Top & Bottom Rebars	Stirrups	Concrete Compressive Strength	Yield Strength of Rebar	Yield Strength of Stirrups
			B × D (mm^2)	t (mm)	- (mm)	- (mm)	f_c\` (MPa)	f_{yb} (MPa)	f_{ys} (MPa)
B1	5F 10F 15F	1 – 5F 6 – 10F 11 – 15F	350×600	150	6 D25	3 D16 – 100	30	490	345
B2	5F 10F 15F	1 – 5F 6 – 10F 11 – 15F	350×600	150	5 D25	3 D16 – 100	30	490	345
B3	10F 15F	1 – 5F 6 – 10F	400×700	150	6 D25	3 D16 – 100	36	490	345
B4	10F 15F	1 – 5F 6 – 10F	400×700	150	5 D25	3 D16 – 100	36	490	345
B5	15F	1 – 5F	450×800	150	6 D25	3 D16 – 100	42	490	345
B6	15F	1 – 5F	450×800	150	5 D25	3 D16 – 100	42	490	345

Table 3. Column section and material properties

No.	Building	Location	Section	Axial Rebars	Hoops	Concrete Compressive Strength	Yield Strength of Rebar	Yield Strength of Hoops
			B ×D (mm^2)	- (mm)	- (mm)	f_c\` (MPa)	f_{yb} (MPa)	f_{ys} (MPa)
C1	5F 10F 15F	1 – 5F 6 – 10F 11 – 15F	700×700	20 D25	4 D16 –100	30	490	345
C2	5F 10F 15F	1 – 5F 6 – 10F 11 – 15F	600×600	16 D25	4 D16 – 100	30	490	345
C3	10F	1 – 5F	800×800	20 D25	4 D16 – 100	36	490	345
C4	10F 15F	1 – 5F 6 – 10F	700×700	16 D25	4 D16 – 100	36	490	345
C5	15F	1 – 5F	900×900	20 D25	4 D16 – 100	42	490	345
C6	15F	1 – 5F	800×800	16 D25	4 D16 – 100	42	490	345
C7	15F	6 – 10F	800×800	16 D25	4 D16 – 100	36	490	345
C8	15F	10 – 15F	700×700	16 D25	4 D16 – 100	30	490	345

The base isolation system incorporated a combination of devices, including elastic sliding bearings (ESB), lead rubber bearings (LRB), and natural rubber bearings (NRB), as shown in Figure 2-c. The dimensions of each device were determined based on the long-term axial forces exerted by the columns, ensuring these forces remained within each device's capacity according to the manufacturer's specifications [33, 34]. The design parameters for the base isolators are summarized in Table 4.

Table 4. Design parameters of base isolation devices according to Bridgestone [33] and Oiles [34] catalogs

Device	ID	Building	Initial Stiffness	Yield Strength	Second Stiffness	Design Displacement	Effective Stiffness	Vertical Stiffness
			K_0 (kN/mm)	F_y (kN)	K_2 (mm)	D_d (mm)	K_{eff} (kN/mm)	K_v (kN/mm)
ESB	SL040GC	5F	3.85	253.50	0	450.00	0.56	3290
	SL070GC	10F	7.44	468.00	0	697.50	0.67	6190
	SSR-S-8080R06	15F	65.60	719.30	0	652.50	1.10	78102
LRB	LH060G4	5F	7.14	43.30	0.55	414.80	0.65	1670
	LL060G4	10F	8.82	43.30	0.69	414.40	0.77	2070
	LH070G4	15F	9.63	67.80	0.74	483.20	0.87	2250
NRB	NS070N3	5F, 10F	0.80	-	-	451.20	0.80	2470
	NS085N3	15F	0.98	-	-	547.20	0.98	3000
	SL040GC	5F	3.85	253.50	0	450.00	0.56	3290

Additionally, oil dampers were installed to control bearing displacement and increase the damping capacity of the base isolation system. The required relief force for these dampers was set at 40% of the total yield force capacity of the base isolation devices. The number of dampers needed was calculated by dividing the required relief force by each device's relief force capacity, as specified in the manufacturer's catalog [35]. The design parameters for the oil dampers are presented in Table 5.

Table 5. Design parameters of oil damper according to Kawakin catalog [35]

ID	Building	Initial Damping	Second Damping	Relief Force	Relief Velocity
		C_1 (kN.s/mm)	C_2 (kN.s/mm)	F_R (kN)	V_R (mm/s)
KYM-750-B	5F, 10F	1.875	0.127	600	320
KYM-1000-B	15F	2.500	0.170	800	320

2.3. Cone Model Approach

The sway and rocking characteristics of a layered soil system were calculated using the cone model approach. For a foundation situated on layered soil, each layer at depth d has several properties, such as soil unit weight (ρ), shear modulus (G), elastic modulus (E), Poisson's ratio (v), and damping ratio (c). This model is based on the assumption that the soil beneath a massless circular foundation act as an elastic semi-infinite medium that responds to dynamic loading through a series of truncated conical bars radiating outward from the load application point (apex) [17]. The cross-sectional area of the cone increases with depth. Accordingly, the truncated cone area (A) is equal to the foundation area (A_0) multiplied by the square of the ratio between the truncated cone depth (z) and the foundation depth (z_0) from the apex. The truncated cone and foundation areas are represented by a circular area involving the radius of the cone at i^{th} layer (r_i) and at (i – 1)th layer (r_{i-1}), as well as the foundation radius (r_0), as illustrated in Figure 3.

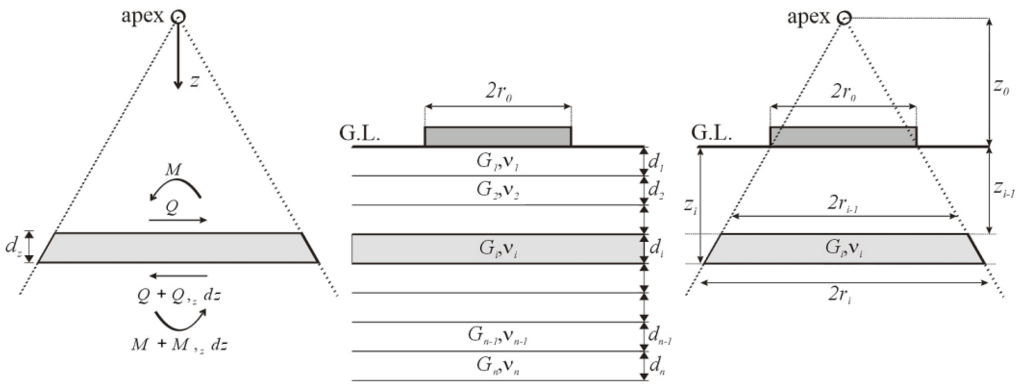

Figure 3. Truncated semi-infinite shear and rocking cone model [17, 18]

In the sway model case, the shear stress (Q) acting on the bottom and top of the truncated cone is equivalent. Meanwhile, the strain response due to the applied force can be presented as the differential form of displacement with respect to the truncated cone depth ($\partial u/\partial z$). It will result in higher-order components with a very small value that can be ignored. At the boundary condition, the lateral displacement (U) occurs at the ground surface; otherwise, it is 0 at the depth of z. If the depth of the truncated cone is assumed to be infinite, the sway stiffness (K_H) can be expressed through Equation 1 by dividing the shear stress at the ground surface (Q_0) by the lateral displacement at the ground surface (U). Additionally, the static sway stiffness for a homogeneous half-space, explained by Wolf [18], is shown in Equation 2. The foundation distance from the apex (z_0) is obtained by equating the cone model stiffness in Equation 1 with the stiffness for a homogeneous half-space in Equation 2, resulting in Equation 3.

$$K_H = -\frac{Q_0}{U} = \frac{\pi r_0^2 G}{z_0} \tag{1}$$

$$K_X = \frac{8Gr_0}{2-\nu} \tag{2}$$

$$z_0 = \frac{\pi r_0(2-\nu)}{8} \tag{3}$$

The truncated cone area increases as the soil depth increases, so the sway stiffness at i^{th} layer (K_H^i) can be expressed through Equation 4, where G_1, G_i, G_n are the shear modulus at the first layer, i^{th} layer, and n^{th} layer, z_i and z_{i-1} are the depth at i^{th} and $(i-1)^{th}$ layer, respectively. In the case of layered soil, each layer is linked in a series system, so the total sway series stiffness (K_{hb}) can be written in Equation 5. Meanwhile, the variable α in Equations 6 and 7 represents impedance factor of sway at i^{th} (α_i) or n^{th} (α_n) layer.

$$K_H^i = \frac{\pi r_0^2 G_1}{z_0}\left(\frac{G_i}{G_1}\right)\frac{z_i z_{i-1}}{z_0(z_i - z_{i-1})} \tag{4}$$

$$K_{hb} = \frac{1}{\sum_{i=1}^{n}(1/\alpha_i)} K_H \tag{5}$$

$$\alpha_i = \left(\frac{G_i}{G_1}\right)\frac{z_i z_{i-1}}{z_0(z_i - z_{i-1})} \tag{6}$$

$$\alpha_n = \left(\frac{G_n}{G_1}\right)\frac{z_{n-1}}{z_0} \tag{7}$$

In the case of rocking motion, the rocking stiffness of cone model (K_R) in Equation 16 can be obtained by implementing the same concept as in sway motion where the moment (M) acting on the bottom and top of foundation are equivalent. Meanwhile, the Equation for static rocking stiffness on homogeneous soil (K_θ) is shown in Equation 8 according to Wolf [18] and Architectural Institute of Japan (AIJ) [36]. Equalizing Equations 8 and 9 will result in the foundation distance from the apex (z_0) in Equation 10. Furthermore, the series rocking stiffness of layered soil is written in Equations 11 to 14, where K_R^i is rocking stiffness at i^{th} layer, K_{rb} is total series rocking stiffness, E_1 is elastic modulus of soil at the first layer, E_n is elastic modulus at n^{th} layer, ν_1 is the Poisson's ratio at the first layer, while α_{ri} and α_{rn} are impedance factor of rocking at i^{th} and n^{th} layer, respectively.

$$K_R = \frac{3\pi r_0^4 E}{4z_0} \tag{8}$$

$$K_\theta = \frac{8Gr_0^3}{3(1-\nu)} \tag{9}$$

$$z_0 = \frac{9\pi r_0(1-\nu^2)}{16} \tag{10}$$

$$K_R^i = \frac{3\pi r_0^4 E_1}{4z_0}\left(\frac{E_i}{E_1}\right)\frac{z_i^3 z_{i-1}^3}{z_0^3(z_i^3 - z_{i-1}^3)} \tag{11}$$

$$K_{rb} = \frac{1}{\sum_{i=1}^{n}(1/\alpha_{ri})}\frac{4r_0^3 E_1}{3(1-\nu_1^2)} \tag{12}$$

$$\alpha_{ri} = \left(\frac{E_i}{E_1}\right)\frac{z_i^3 z_{i-1}^3}{z_0^3(z_i^3 - z_{i-1}^3)} \tag{13}$$

$$\alpha_{rn} = \left(\frac{E_n}{E_1}\right)\left(\frac{z_{n-1}}{z_0}\right)^3 \tag{14}$$

On the other hand, the ground motion acting on the massless rigid foundation leads to wave propagation downwards from the foundation, which is called radiation damping [10, 17, 37]. The motion acting on the ground surface is equal to the foundation motion, so only the wave travelling away from the structure exists in the soil layer. The derivation of the radiation damping formula was presented by Shibata [37]. Meanwhile, the radiation damping due to sway (c_H) and rocking (c_R) are shown in Equations 15 to 17, where A_0 and I_0 are the circular foundation's section area and moment of inertia, V_{La} is Lysmer's analog velocity, and V_s is shear wave velocity.

$$c_H = \rho V_s A_0 \tag{15}$$

$$c_R = \rho V_{La} I_0 \tag{16}$$

$$V_{La} = \frac{3.4 V_S}{\pi(1-\nu)} \tag{17}$$

The sway-rocking model applied on a base-isolated building is depicted in Figure 4. The cone model method was applied, and the sway-rocking parameters were calculated by STERA 3D v11.5. The input soil properties for hard, medium, and soft soils are summarized in Table 6. The cone model parameters are presented in Table 7.

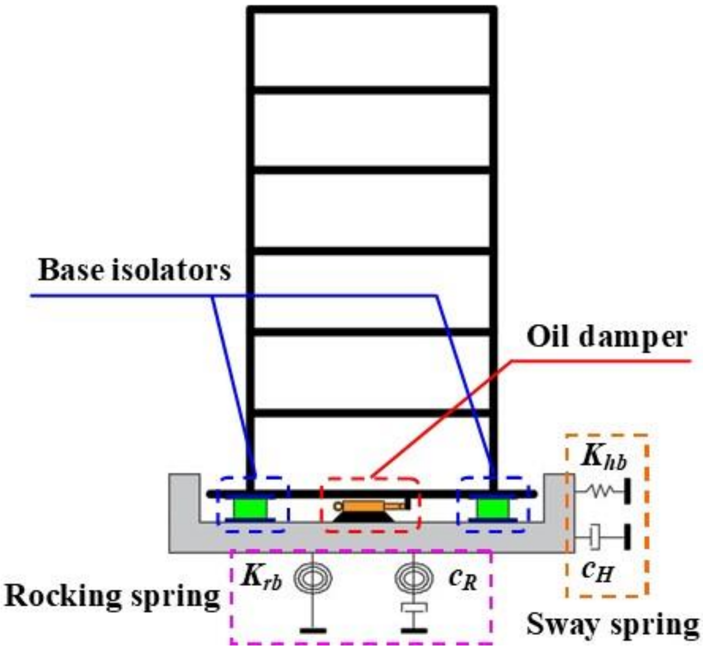

Figure 4. Sway-rocking model applied on base-isolated building

Table 6. Three soil properties according to Caltrans' soil classification [31]

Layer	Soil Unit Weight ρ (kN/m³)	Layer Thickness d_i (m)	Shear Wave Velocity, V_s Hard (m/s)	Medium (m/s)	Soft (m/s)
1	16.0	3	340	170	100
2	17.0	7	430	220	110
3	17.5	6	520	260	130
4	18.0	14	700	350	170
Bedrock	23.6	∞	1000	1000	1000

Table 7. Sway and rocking spring parameters

Building	Base Dimension $(B \times D \times t)$ (m³)	Soil Type	Sway Stiffness K_{hb} (kN/m)	Sway Radiation Damping c_H (kN.s/m)	Rocking Stiffness K_{rb} kNm/rad	Rocking Radiation Damping c_R kNm.s/rad
5F	22.5×22.5×0.6	Hard	1.14×10^7	1.20×10^6	1.28×10^9	7.79×10^7
		Medium	2.97×10^6	1.20×10^6	3.29×10^8	7.79×10^7
		Soft	8.58×10^5	1.20×10^6	9.52×10^7	7.79×10^7
10F	22.5×22.5×0.8	Hard	1.16×10^7	1.20×10^6	1.32×10^9	7.79×10^7
		Medium	3.03×10^6	1.20×10^6	3.37×10^8	7.79×10^7
		Soft	8.70×10^5	1.20×10^6	9.71×10^7	7.79×10^7
15F	22.5×22.5×1.0	Hard	1.18×10^7	1.20×10^6	1.35×10^9	7.79×10^7
		Medium	3.10×10^6	1.20×10^6	3.46×10^8	7.79×10^7
		Soft	8.83×10^5	1.20×10^6	9.89×10^7	7.79×10^7

2.4. Spectrum-Matched Ground Motions

Three artificial ground motions with different earthquake phases as summarized in Table 8 were generated using STERA WAVE v1.0 [38] to match the design response spectrum of level 2 earthquake intensity (life safety) [28]. The soil amplification factor to the engineering bedrock was considered in each soil condition based on the equivalent single-soil layer method to represent multilayer soil properties [36]. The matched-spectra of each ground motion to the target response spectrum considering hard soil (RS-Hard), medium soil (RS-Medium), and soft soil (RS-Soft) amplifications are presented in Figures 5-a to 5-c. The time histories of generated ground motions are presented in Figures 5-d to 5-f.

Table 8. Selected ground motions for nonlinear time history analysis

No.	ID	Phase Information	Year	Component
1	Art-EC	El Centro	1940	North-South (NS)
2	Art-Kobe	Kobe	1995	North-South (NS)
3	Art-Random	Random	-	-

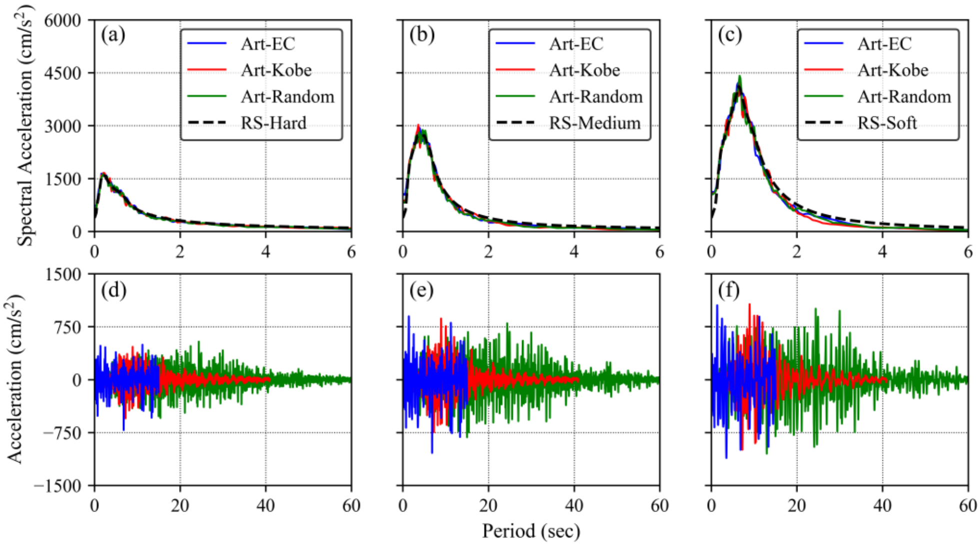

Figure 5. Spectral matching results: (a) response spectrum of hard soil, (b) medium soil, and (c) soft soil, (d) ground motion of hard soil, (e) medium soil, and (f) soft soil

2.5. Modeling Method in STERA 3D

Figure 6 illustrates the three-dimensional frame models generated using STERA 3D v11.5 [27] to simulate base-isolated buildings of varying heights. Beams and columns were defined as line elements using three-dimensional beam-column formulations that included axial, torsional, nonlinear bending, and nonlinear shear springs. The flexural behavior of beams and columns followed a tri-linear hysteretic loop based on the Takeda model [39], which represents cracking, yielding, and nonlinear states while accounting for degradation. Beam-column connections were assumed to be rigid, with shear deformation in the connection area neglected. The floor diaphragm was modeled as rigid for in-plane deformation. Additionally, floor mass was assumed to be lumped at the center of gravity on each story.

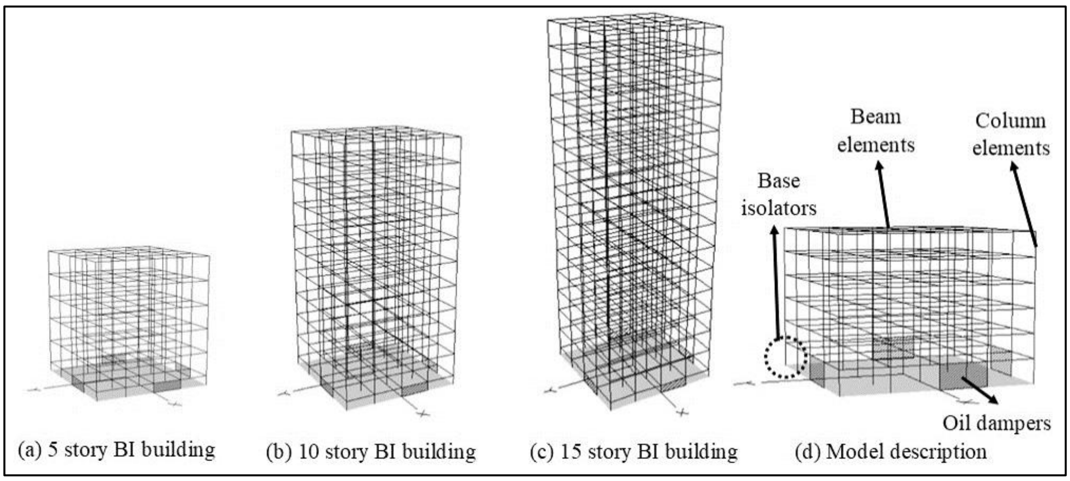

Figure 6. Base-isolated building models in STERA 3D v11.5

Ground springs were used to model sway and rocking springs based on the cone model and were applied to the building's basement, where the floor diaphragm was restrained at the center of gravity in all degrees of freedom except in the sway and rocking directions. The base isolation system was idealized with link elements that considered only the lateral and vertical stiffness. Lead rubber bearings (LRB) and elastic sliding bearings (ESB) were modeled with bilinear curves, while natural rubber bearings (NRB) were represented using an elastic model. The oil damper was modeled as a line element and its force-velocity relationship was represented using the Maxwell model, which consists of an elastic spring and viscous dashpot in series, as described by Papanicolaou & Zaoutsos [40].

3. Results and Discussion

3.1. Introduction

This study involves two primary cases: base-isolated (BI) building models with and without considering SSI effects. Each case was subjected to three ground motion events, accounting for the amplification factor due to soil wave propagation across different soil profiles. Aspect ratios of 1.58, 3.15, and 4.73 were used to represent the slenderness of 5-, 10-, and 15-story buildings, respectively, calculated by dividing the total building height (H) by the equivalent radius of foundation (r_0). The analysis results, including the effects of SSI on the natural period, story displacement and drift, story acceleration, story shear, and base rotation, are presented and discussed.

3.2. Natural Period

Modal analysis was conducted to evaluate the impact of SSI on the natural period of base-isolated buildings. As illustrated in Figure 7, BI buildings with higher aspect ratios were more affected by SSI in the first and second modes. For 5-story buildings (aspect ratio of 1.58), the first mode natural periods were 2.799 sec, 2.803 sec, 2.813 sec, and 2.847 sec for BI buildings without SSI and with hard, medium, and soft soils, respectively. Conversely, for 15-story buildings (aspect ratio of 4.73), the first mode natural periods were 4.027 sec, 4.056 sec, 4.142 sec, and 4.429 sec for BI buildings without SSI and with hard, medium, and soft soils, respectively.

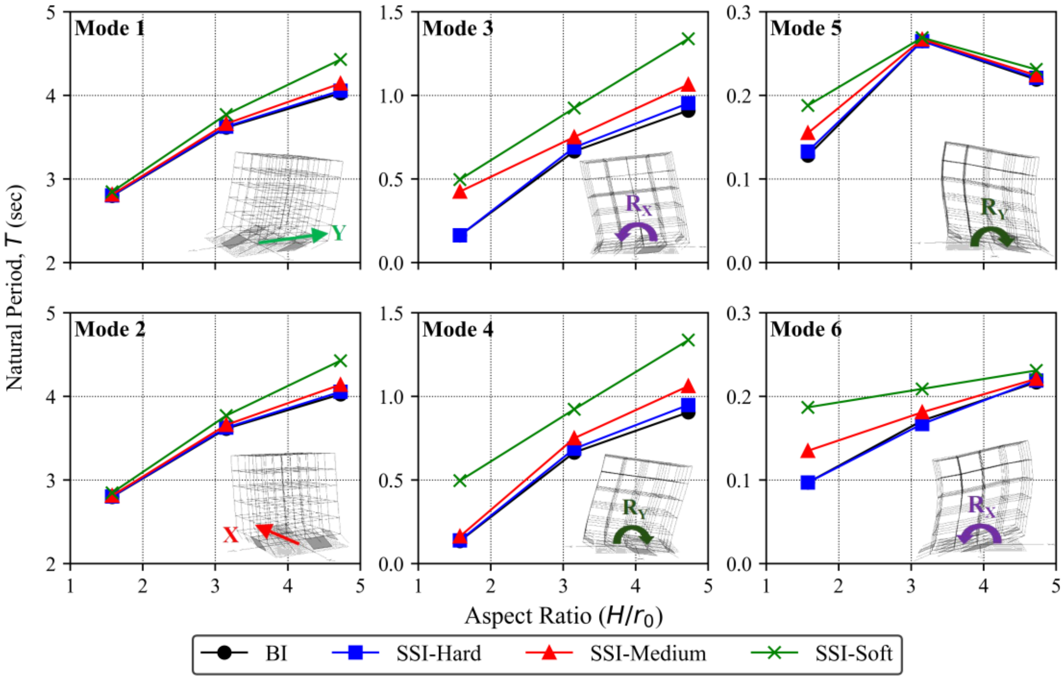

Figure 7. Natural period of BI buildings comparison to the aspect ratio (H/r)

A similar trend was observed in the second mode, with the natural period gradually increasing as the soil became softer. This indicates that the aspect ratio significantly influences the impact of SSI. Figure 8 further confirmed that the increase in the natural period was more pronounced for BI buildings with higher aspect ratios. This was shown by the percentage increase of the natural period of BI buildings with SSI (T_{SSI}) relative to those without SSI (T_{BI}), calculated as $(T_{SSI} - T_{BI})/T_{BI}$. The results showed that for the first and second modes, the natural period of the 5-story building increased by 0.1%, 0.5%, and 1.7% due to hard, medium, and soft soil effects, respectively. In contrast, the natural period of the 15-story building increased by 0.7%, 2.9%, and 10% for the same soil conditions. These findings align with studies by Alavi and Alidoost [5] and Hatami et al. [6], which stated that the greatest natural period increase was shown by BI buildings with an aspect ratio of 4.0 on soft soil, that was up to 26%. Overall, the results indicate that while hard soil has a minimal effect on the natural period, medium, and soft soils contribute to more significant increases.

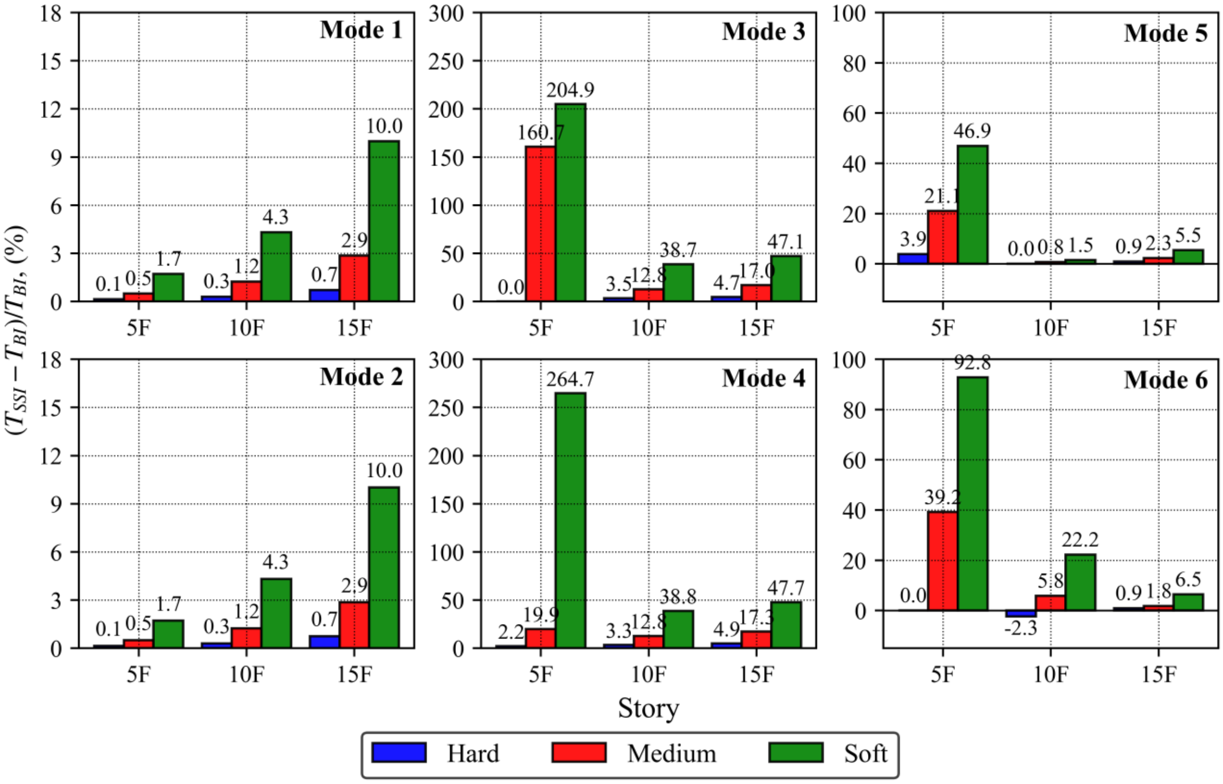

Figure 8. Relative natural period of BI buildings with and without considering SSI

At higher modes, where rotational modes occurred, the effects of medium and soft soil were more pronounced in the 5-story model compared to the 10- and 15-story models. From mode 3 to mode 6, the natural period of the 5-story model increased significantly due to the influence of medium and soft soils, while hard soil had a negligible effect on the natural period. It was observed that, in mode 3, the natural period of the 5-story building was 0.163 seconds without considering SSI, and increased to 0.163 seconds, 0.425 seconds, and 0.497 seconds when SSI with hard, medium, and soft soils were considered, respectively. Meanwhile, the natural period of the 15-story building without SSI was 0.91 seconds and increased to 0.953 seconds, 1.065 seconds, and 1.339 seconds for hard, medium, and soft soils, respectively. This period increase was also confirmed in Figure 8, where the greatest increase in mode 3 was observed in the 5-story model, with changes of 0.0%, 160.7%, and 204.9%. In contrast, the natural period of the 15-story building increased by 4.7%, 17.0%, and 47.1% for hard, medium, and soft soils, respectively. These findings align with the study by Jennings and Bielak [41], who noted that SSI has a smaller effect on the natural period of tall buildings at higher modes. Conversely, the natural period of shorter buildings increased in higher modes as the soil became softer. This phenomenon attributed to the rocking of the building rather than the swaying of the base mass [41].

3.3. Story Displacement and Drift

Figure 9 shows the average story displacement of 5-, 10-, and 15-story BI buildings under three input ground motions. It was observed that SSI had minimal impact on the story displacement of the 5-story and 10-story buildings, whereas its effects were more pronounced for the 15-story building, particularly due to soft soil. Additionally, isolation layer displacement was a crucial indicator for ensuring safety against displacement demands during earthquakes. Therefore, the design displacement of the LRB (maximum base isolator displacement) from Table 4 was used, as it had the lowest design displacement among all devices. In this context, the largest displacement was observed due to the soft soil effect but remained below the maximum allowable base isolator displacement. Specifically, the isolation layer displacements for the 5-story building without and with the soft soil effect were 35.76 cm and 35.65 cm, respectively. For the 10-story building, the results were 28.32 cm without and 29.15 cm with the soft soil effect. Similarly, for the 15-story building, the displacements were 26.75 cm without and 27.66 cm with the soft soil effect. Figure 10 exhibits the percentage changes of the top story and isolation layer displacements of BI buildings with SSI (δ_{SSI}) relative to those without SSI (δ_{BI}), calculated as $(\delta_{SSI} - \delta_{BI})/\delta_{BI}$. The results indicate that the SSI effect slightly increased the isolation layer displacement of the 10- and 15-story buildings by 2.90% and 3.40% due to the soft soil, while the change in the 5-story building was negligible. Additionally, the hard and medium soil cases showed negligible changes in isolation layer displacement for all buildings, with values below 1.0%.

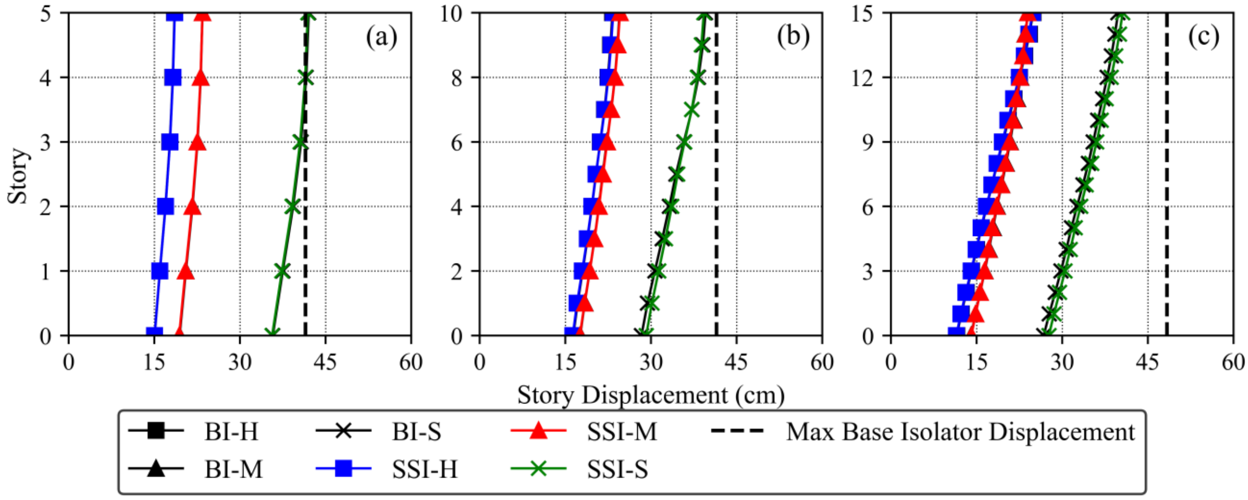

Figure 9. Average story displacement of BI buildings: (a) 5-story, (b) 10-story, and (c) 15-story

The top story displacement was not significantly affected by SSI, as shown in Figure 9. The largest displacement response was observed in the BI building on soft soil, which was comparable to that of the BI building without SSI. For example, the top story displacements of the 5-story building were 42.06 cm without and 41.90 cm with the soft soil effect. The 10-story building showed displacements of 39.54 cm without and 39.25 cm with the soft soil effect. For the 15-story building, the top story displacements were 39.77 cm without and 40.58 cm with the soft soil effect. These results indicate that SSI slightly influenced the top story displacement across all BI building models. Figure 10 shows that the maximum rate of increase was 2.0% for the 15-story building, while the 5- and 10-story buildings experienced slight decreases of 0.40% and 0.70%, respectively. These outcomes align with the study by Yanik and Ulus [8], which noted that the effect of SSI on story displacement was more pronounced under soft soil conditions and could reduce the top story displacement of BI buildings, although some increases were observed in certain earthquake response cases.

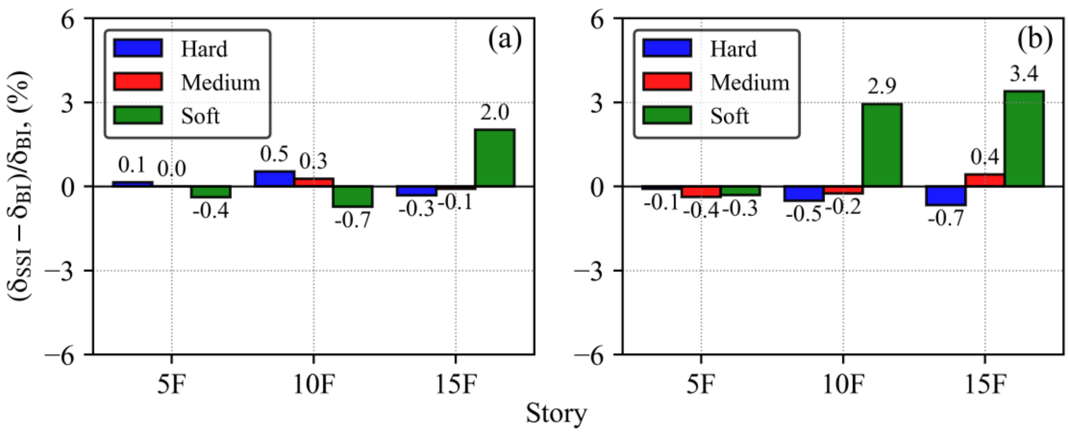

Figure 10. (a) Relative top story displacement and (b) Relative isolation layer displacement of BI buildings with and without considering SSI

Figure 11 presents the average story drift of 5-, 10-, and 15-story BI buildings, while Figure 12 shows the rate of story drift changes due to the effect of SSI. It is calculated as $(\Delta_{SSI} - \Delta_{BI})/\Delta_{BI}$, where Δ_{SSI} is the story drift of BI buildings with SSI and those without SSI is represented by Δ_{BI}. Story drift is defined as the angle between the lateral relative displacement of each story and the story below, divided by the story height. If a particular story exceeds the story drift limit set by code provisions, it may require stiffening. In this study, the largest story drift occurred due to the soft soil effect across all building cases. For the 5-story building, the soft soil reduced the story drift by 0.40%, from 4.75×10^{-3} to 4.72×10^{-3} without and with the soft soil effect, respectively. In the 10-story building, the story drift decreased by up to 12.10%, from 4.48×10^{-3} to 3.94×10^{-3} due to the soft soil. The most significant reduction of 24.60% was observed in the 15-story building, where the story drift decreased from 4.94×10^{-3} to 3.72×10^{-3}. While the soft soil consistently reduced story drift, the hard and medium soils generally led to increases, as shown in Figure 12. The results indicated that hard soil increased the story drift of the 5-, 10-, and 15-story buildings by up to 2.90%, 4.00%, and 1.90%, respectively. Meanwhile, the medium soil caused an increase in story drift for the 5- and 10-story buildings by up to 2.90% and 5.10%, respectively, but resulted in a 6.70% reduction in the 15-story building.

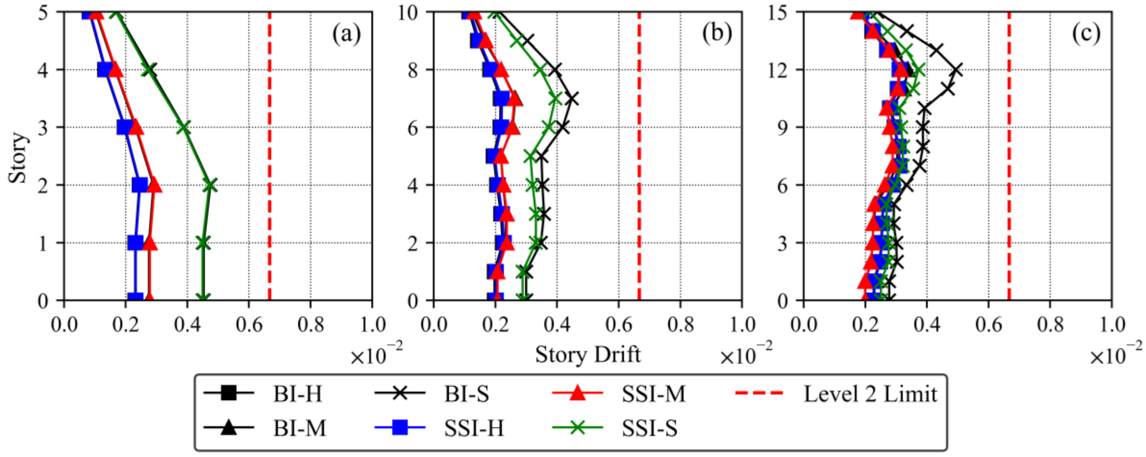

Figure 11. Average story drift of BI buildings: (a) 5-story, (b) 10-story, and (c) 15-story

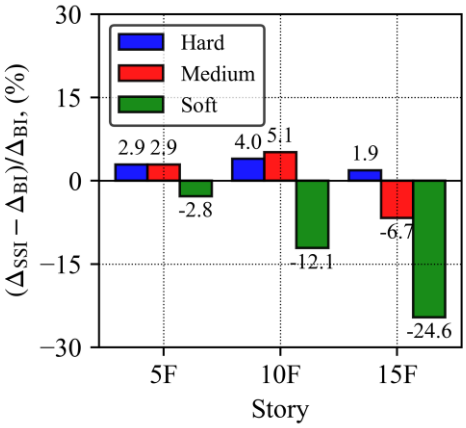

Figure 12. Maximum relative story drift of BI buildings with and without considering SSI

3.4. Story Acceleration

The effect of SSI on the story acceleration of BI buildings was more pronounced in medium and soft soil conditions, especially for the 10- and 15-story buildings. In these cases, the most significant acceleration occurred at the top stories and isolation layers. Similar results were found by Zhuang et al. [42] in an experimental study, where story accelerations were lower in the middle stories compared to the top and bottom stories.

As shown in Figure 13, the largest acceleration in the 5-story building was observed at the isolation layer and significantly reduced from 331.27 cm/s² without SSI to 318.33 cm/s² with SSI. Similarly, in the 10-story building, the peak acceleration of 267.37 cm/s² at the isolation layer was reduced to 249.10 cm/s² due to the soft soil effects. For the 15-story building, the highest acceleration at the isolation layer was 404.37 cm/s² without SSI, decreasing to 351.30 cm/s² with the consideration of soft soil effects.

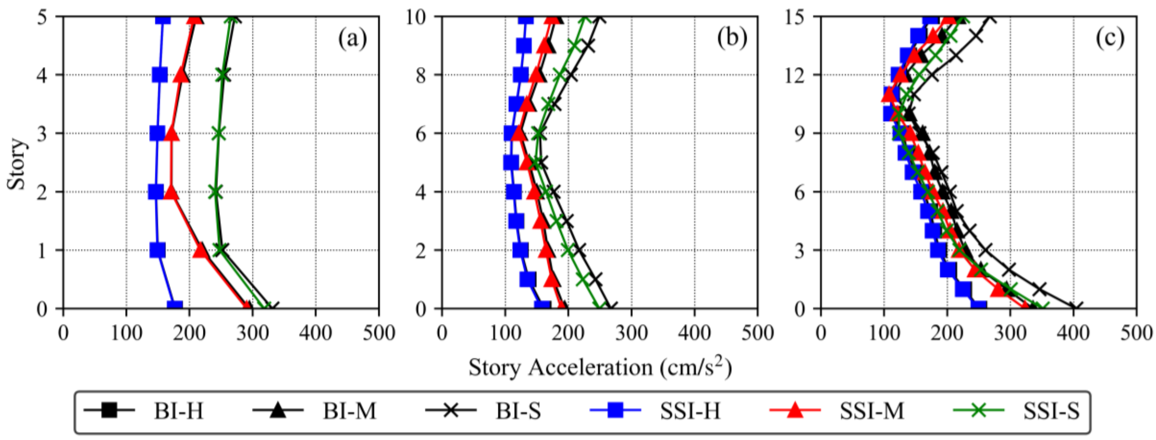

Figure 13. Average story acceleration of BI buildings: (a) 5-story, (b) 10-story, and (c) 15-story

Figure 14 clearly shows the reduction rates due to all soil cases, with the largest reduction observed in the soft soil for the 5-, 10-, and 15-story buildings. It is calculated using $(a_{SSI} - a_{BI})/a_{BI}$, where a_{SSI} is the story acceleration of BI buildings with SSI and those without SSI is represented by a_{BI}. In the 5-story building, acceleration reductions of 0.40%, 1.40%, and 3.90% were recorded for hard, medium, and soft soils, respectively. Greater reductions were noted in the 10-story building, with decreases of 1.90%, 2.60%, and 6.80% for hard, medium, and soft soil conditions. Similarly, the 15-story building experienced reductions of 2.30%, 10.20%, and 22.50% due to hard, medium, and soft soils, respectively. This indicates that story acceleration reduction increased as the soil became softer. These findings align with Yanik and Ulus [8], who reported that SSI could reduce story acceleration, with the most significant effects seen in soft soil conditions. The current study demonstrated that all soil types could reduce story acceleration, although the reduction rate varied depending on story height and soil characteristics. Specifically, the reduction rate increased with greater story height and softer soil conditions.

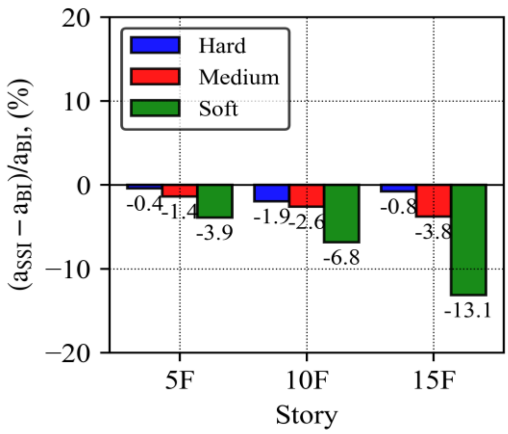

Figure 14. Average story acceleration of BI buildings: (a) 5-story, (b) 10-story, and (c) 15-story

3.5. Story Shear

In this section, the base and story shears of BI buildings with and without SSI are evaluated. To prevent overstressing the structural elements from lateral earthquake forces at each story, a shear capacity curve is plotted in Figure 15. This curve was calculated using pushover analysis for a fixed-base building and compared with the story shears of the BI building under earthquake excitations. The results in Figure 15 show that the base and story shears did not exceed the shear capacity, indicating that the building is safe against shear forces from the input earthquakes.

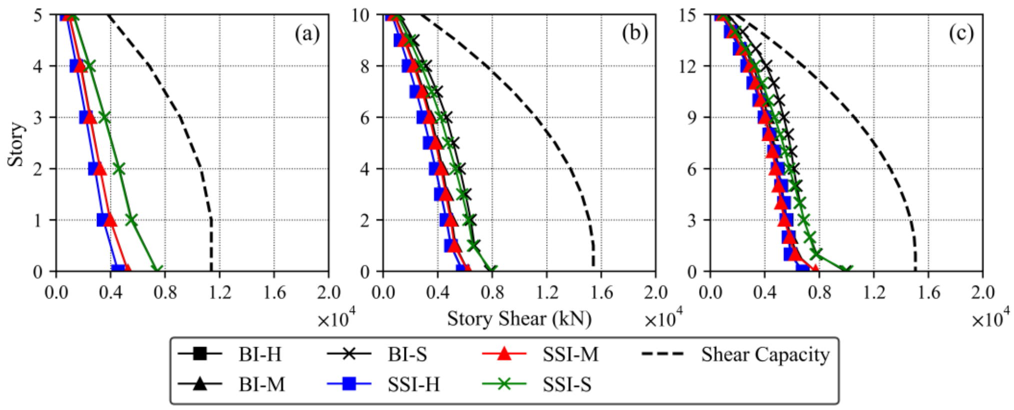

Figure 15. Average story shear of BI buildings: (a) 5-story, (b) 10-story, and (c) 15-story

The effect of SSI on base shear is illustrated in Figure 15. The results indicate that the impact of SSI was negligible for BI buildings on hard and medium soil, while a slight increase was noted for buildings on soft soil. For example, the base shear of the 5-story building was 7417.67 kN without SSI and 7401.67 kN with the soft soil effect. In the 10-story building, base shears were 7841.00 kN without and 7964.67 kN with soft soil. Similarly, the base shears for the 15-story building were 9920.00 kN without and 10053.30 kN with the soft soil effect.

Furthermore, the rate of change in base shear is presented in Figure 16-a, calculated using $(V_{SSI} - V_{BI})/V_{BI}$, where V_{SSI} is the base or story shear of BI buildings with SSI and V_{BI} represents those without SSI. The results indicate that SSI caused a slight reduction in the 5-story building's base shear, with decreases of 0.10%, 0.30%, and 0.20% for hard, medium, and soft soil, respectively. Similarly, in the 10-story building, reductions of 0.40% and 0.30% were noted for hard and medium soil, while soft soil resulted in a 1.60% increase. In the 15-story building, SSI led to reductions of 0.50% and 0.01% for hard and medium soil, but soft soil caused a 1.30% increase.

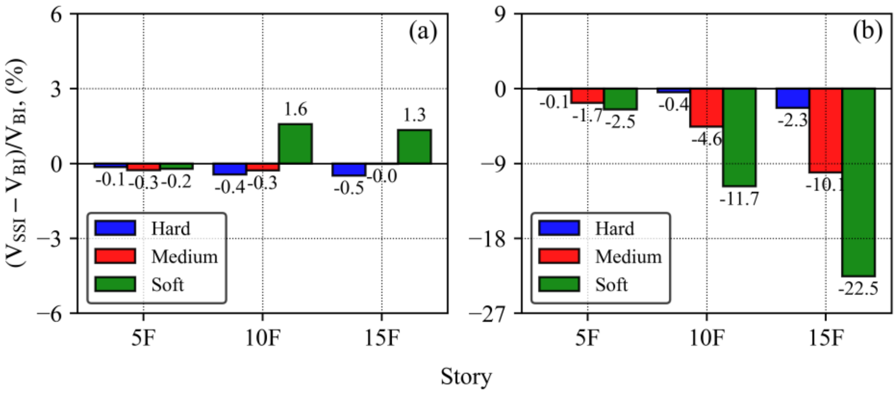

Figure 16. Relative maximum (a) base shear and (b) story shear of BI buildings with and without considering SSI

These findings show that SSI caused only minor changes in base shear. In comparison, Alavi & Alidoost [5] showed a greater base shear reduction in response spectrum analysis for a lumped mass model as the soil became softer. However, a finite element analysis by Forcellini et al. [9] yielded similar results to the current study, showing that SSI did not significantly reduce the base shear of BI buildings. This was because soft soil induced large shear strain during an earthquake, which was absorbed by the isolation devices, resulting in larger base shear at the isolation layer [9].

On the other hand, the effect of SSI on story shear is more pronounced with soft soil, particularly in the 10- and 15-story BI buildings. Figure 15 shows that the story shears of the 5-story buildings with and without SSI remained identical. The story shear reduction is presented in Figure 16-b, calculated using the same method described previously. The largest story shear reduction in the 5-story building was 2.50% at the fifth story, decreasing from 1279.67 kN without SSI to 1247.67 kN with SSI on soft soil. For the 10-story building, the largest reduction was 11.70% at the ninth story, dropping from 2221.33 kN without SSI to 1960.33 kN with soft soil effects. In the 15-story building, the most significant reduction of 22.50% occurred at the fourteenth story, where shear decreased from 2379.00 kN without SSI to 1842.67 kN with SSI on soft soil. Figure 16-b also indicates that increased soil softness led to greater story shear reductions. For instance, in the 15-story building, the reduction rates for hard, medium, and soft soils were 2.30%, 10.10%, and 22.50%, respectively.

3.6. Base Rotation (Rocking Effect)

The rocking effect of BI buildings may cause additional displacement in the superstructure, represented by the rotation angle at the base. To examine the impact of the base isolation system on rocking behavior, non-isolated (NI) buildings with the same structural and soil spring properties as the BI buildings were analyzed. As shown in Figure 17, the base-isolated model exhibited smaller rotation angles compared to the non-isolated model in all cases. This reduction is due to the additional damping provided by the base isolation system, which dissipates a substantial amount of earthquake energy, thereby minimizing the energy transmitted to the superstructure. Furthermore, the base isolation system creates a more uniform distribution of inertia forces in the superstructure, reducing the rotational angle in base-isolated buildings, as the mass moment of inertia is lower compared to non-isolated buildings. This indicates that the base isolation system effectively reduces rocking behavior in 5-, 10-, and 15-story BI buildings.

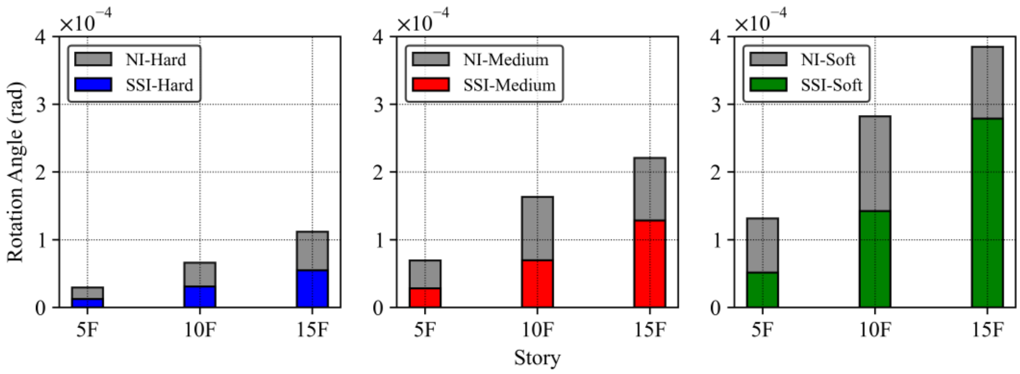

Figure 17. Average base rotation of non-isolated (NI) and BI buildings considering SSI

According to Figure 17, the soft soil effect on the BI building resulted in the largest rotation angle compared to hard and medium soils. For instance, the rotation angles of the 5-story building due to hard, medium, and soft soil effects were 0.12×10^{-4} rad, 0.28×10^{-4} rad, and 0.52×10^{-4} rad. In the 10-story building, hard, medium, and soft soils produced rotation angles of 0.31×10^{-4} rad, 0.69×10^{-4} rad, and 1.42×10^{-4} rad. Similarly, in the 15-story building, rotation angles were 0.55×10^{-4} rad, 1.28×10^{-4} rad, and 2.79×10^{-4} rad due to hard, medium, and soft soil effects, respectively. These outcomes align with the experimental study by Zhuang et al. [42], which found that the rotation at the isolation layer and pile cap increased more on soft soil than on hard soil. Furthermore, the current results also demonstrated that increasing building height could amplify the SSI effect, leading to a larger rotation angle. This finding is consistent with the study by Ismail et al. [43], who evaluated the impact of story count on the seismic behavior of mid-rise frame structures. Their results showed that as the number of stories increased, the foundation's rotation angle also increased.

The rotation angle results were also influenced by soil amplification, which increased the amplitude of ground motions, while the low rotational stiffness of the rocking soil spring enhanced soil-structure flexibility, resulting in a larger rotation angle. However, these results were relatively small compared to the angle of the top superstructure displacement relative to the building height, as summarized in Table 9. This implies that the rocking effect did not significantly contribute to an increase in superstructure displacement, as shown in Figure 18. Additionally, rotational mode shapes first appeared at higher modes, starting from mode 3, as shown in Figure 7. Consequently, the contribution of higher modes due to SSI to the rocking effect and superstructure displacement was negligible. This aligns with the findings of Jennings and Bielak [41], who concluded that the effect of SSI on seismic responses predominantly occurs at the fundamental mode rather than at higher modes.

Table 9. Rotation angle of BI building considering SSI effect

Building	Hard SSI Effect (SSI-H)		Medium SSI Effect (SSI-M)		Soft SSI Effect (SSI-S)	
	Base (rad)	Superstructure (rad)	Base (rad)	Superstructure (rad)	Base (rad)	Superstructure (rad)
5F	0.12×10^{-4}	0.18	0.28×10^{-4}	0.20	0.52×10^{-4}	0.31
10F	0.31×10^{-4}	0.18	0.69×10^{-4}	0.17	1.42×10^{-4}	0.25
15F	0.55×10^{-4}	0.22	1.28×10^{-4}	0.16	2.79×10^{-4}	0.22

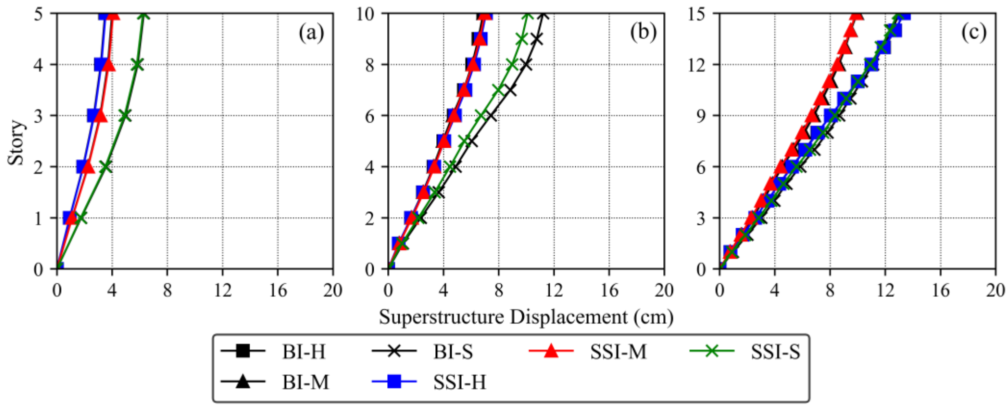

Figure 18. Average superstructure displacement of BI buildings: (a) 5-story, (b) 10-story, and (c) 15-story

4. Conclusions

This study investigated the effects of soil-structure interaction (SSI) on three reinforced concrete base-isolated (BI) buildings with varying story heights. Three soil types were also considered to model the sway and rocking springs using the cone model approach. Based on nonlinear time history and modal analysis, several conclusions were drawn as follows:

- The effects of SSI led to an increase in the natural period of BI buildings. The greatest increases in the first and second modes were observed in the 15-story building, while the smallest increase occurred in the 5-story building. This indicates that in the sway mode pattern, taller, more slender buildings are more affected by SSI. In contrast, the largest increase in higher modes, where the rocking mode pattern is dominant, was seen in the shorter, squat building on soft soil. Additionally, the softer the soil characteristics, the greater the increase in the natural period across all modes.
- The top story displacement was not significantly affected by SSI due to an increase in base displacement, although each story's displacement showed slight variation. However, the presence of a soft soil spring reduced story drift by 2.80%, 12.10%, and 24.60% in the 5-story, 10-story, and 15-story buildings, respectively. In contrast, hard and medium soil conditions tended to slightly increase story drift.

- The presence of SSI reduced story acceleration, with the greatest reduction observed in the BI building on soft soil, followed by those on medium and hard soils, respectively. Additionally, tall and slender buildings were more affected by medium and soft soils compared to shorter, squat buildings.
- SSI had a slight effect on base shear, but it significantly reduced story shear forces, with the reduction being more pronounced in taller, slender buildings on soft soil. Consequently, story force reductions of 2.50%, 11.70%, and 22.50% were observed in the 5-story, 10-story, and 15-story buildings, respectively, due to soft soil. In contrast, the maximum reduction for hard and medium soils did not exceed 10.10% across all building cases.
- The rotational angle was also influenced by the SSI effect, with soft soil producing the largest angle among all soil cases. The rotational angle increased significantly in BI buildings with a higher aspect ratio. Additionally, base-isolated buildings effectively reduced rocking behavior compared to non-isolated buildings.

5. Declarations

5.1. Author Contributions

Conceptualization, A.K.S. and T.S.; methodology, A.K.S.; software, T.S.; formal analysis, A.K.S.; writing—original draft preparation, A.K.S.; writing—review and editing, T.S.; visualization, A.K.S.; supervision, T.S. All authors have read and agreed to the published version of the manuscript.

5.2. Data Availability Statement

The data presented in this study are available in the article.

5.3. Funding

The authors received no financial support for the research, authorship, and/or publication of this article.

5.4. Conflicts of Interest

The authors declare no conflict of interest.

6. References

[1] Naeim, F., & Kelly, J. M. (1999). Design of seismic isolated structures: from theory to practice. John Wiley & Sons, Hoboken, United States. doi:10.1002/9780470172742.

[2] Ziraoui, A., Kissi, B., Aaya, H., & Azdine, I. (2024). Seismic behavior of base-isolated building structures with lead rubber bearings (LRBs). Procedia Structural Integrity, 61, 171–179. doi:10.1016/j.prostr.2024.06.023.

[3] Usta, P. (2021). Investigation of a base-isolator system's effects on the seismic behavior of a historical structure. Buildings, 11(5), 217. doi:10.3390/buildings11050217.

[4] Kramer, S. L. (1996). Geotechnical Earthquake Engineering. Pearson, London, United Kingdom.

[5] Alavi, E., & Alidoost, M. (2012). Soil-structure interaction effects on seismic behavior of base-isolated buildings. 15th World Conference on Earthquake Engineering (WCEE 2012), 24-28 September 2012, Lisbon, Portugal.

[6] Hatami, F., Nademi, H., & Rahaie, M. (2015). Effects of Soil-Structure Interaction on the Seismic Response of Base Isolated in High-Rise Buildings. International Journal of Structural and Civil Engineering Research, 4(3), 237-242. doi:10.18178/ijscer.4.3.237-242.

[7] Du, D. S., Wang, S. G., Liu, W. Q., Shi, S., Lee, C. P., & Xu, J. (2018). Modal property of base-isolated high-rise structure considering soil–structure interaction effect. Advances in Mechanical Engineering, 10(12), 1687814018803808. doi:10.1177/1687814018803808.

[8] Yanik, A., & Ulus, Y. (2023). Soil–Structure Interaction Consideration for Base Isolated Structures under Earthquake Excitation. Buildings, 13(4). doi:10.3390/buildings13040915.

[9] Forcellini, D. (2018). Seismic assessment of a benchmark based isolated ordinary building with soil structure interaction. Bulletin of Earthquake Engineering, 16(5), 2021–2042. doi:10.1007/s10518-017-0268-6.

[10] Cruz, C., & Miranda, E. (2017). Evaluation of soil-structure interaction effects on the damping ratios of buildings subjected to earthquakes. Soil Dynamics and Earthquake Engineering, 100, 183–195. doi:10.1016/j.soildyn.2017.05.034.

[11] Chopra, A. K. (2014). Dynamics of structures theory and applications to earthquake engineering (4th Ed.). Prentice Hall, Hoboken, United States.

[12] Clough, R. W., & Penzien, J. (2003). Dynamic of Structures. McGraw-Hill, New York, United States.

[13] Lamb, H. (1904). I. On the propagation of tremors over the surface of an elastic solid. Philosophical Transactions of the Royal Society of London. Series A, Containing papers of a mathematical or physical character, 203(359-371), 13. doi:10.1098/rsta.1904.0013.

[14] Poulos, H. G., & Davis, E. H. (1974). Elastic solutions for soil and rock mechanics. John Wiley & Sons, Hoboken, United States.

[15] Hadjian, A. H., Luco, J. E., & Tsai, N. C. (1974). Soil-structure interaction: Continuum or finite element? Nuclear Engineering and Design, 31(2), 151–167. doi:10.1016/0029-5493(75)90138-7.

[16] Wolf, J. P., & Deeks, A. J. (2004). Cones to model foundation vibrations: Incompressible soil and axi-symmetric embedment of arbitrary shape. Soil Dynamics and Earthquake Engineering, 24(12), 963–978. doi:10.1016/j.soildyn.2004.06.016.

[17] Wolf, J. P., & Deeks, A. J. (2004). Foundation vibration analysis: A strength of materials approach. Elsevier, Butterworth-Heinemann, Oxford, United Kingdom.

[18] Wolf, J. P. (1994). Foundation vibration analysis using simple physical models. Pearson Education, London, United Kingdom.

[19] Bapir, B., Abrahamczyk, L., Wichtmann, T., & Prada-Sarmiento, L. F. (2023). Soil-structure interaction: A state-of-the-art review of modeling techniques and studies on seismic response of building structures. Frontiers in Built Environment, 9. doi:10.3389/fbuil.2023.1120351.

[20] Pradhan, P. K., Baidya, D. K., & Ghosh, D. P. (2004). Dynamic response of foundations resting on layered soil by cone model. Soil Dynamics and Earthquake Engineering, 24(6), 425–434. doi:10.1016/j.soildyn.2004.03.001.

[21] Gazetas, G. C., & Roesset, J. M. (1979). Vertical Vibration of Machine Foundations. Journal of the Geotechnical Engineering Division, 105(12), 1435–1454. doi:10.1061/ajgeb6.0000899.

[22] Meek, J. W., & Wolf, J. P. (1993). Why cone models can represent the elastic half-space. Earthquake Engineering & Structural Dynamics, 22(9), 759-771. doi:10.1002/eqe.4290220903.

[23] Bararnia, M., Hassani, N., Ganjavi, B., & Ghodrati Amiri, G. (2018). Estimation of inelastic displacement ratios for soil-structure systems with embedded foundation considering kinematic and inertial interaction effects. Engineering Structures, 159, 252–264. doi:10.1016/j.engstruct.2018.01.002.

[24] Hassani, N., Bararnia, M., & Ghodrati Amiri, G. (2018). Effect of soil-structure interaction on inelastic displacement ratios of degrading structures. Soil Dynamics and Earthquake Engineering, 104, 75–87. doi:10.1016/j.soildyn.2017.10.004.

[25] Lu, Y., Hajirasouliha, I., & Marshall, A. M. (2018). An improved replacement oscillator approach for soil-structure interaction analysis considering soft soils. Engineering Structures, 167, 26–38. doi:10.1016/j.engstruct.2018.04.005.

[26] Ganjavi, B., Gholamrezatabar, A., & Hajirasouliha, I. (2019). Effects of soil-structure interaction and lateral design load pattern on performance-based plastic design of steel moment resisting frames. Structural Design of Tall and Special Buildings, 28(11), e1624. doi:10.1002/tal.1624.

[27] Saito, T. (2024). Structural Earthquake Response Analysis 3D, (STERA 3D Version 11.5). Earthquake Disaster Engineering Research Laboratory, Toyohashi University of Technology, Toyohashi, Japan. Available online: https://rc.ace.tut.ac.jp/saito/software-e.html#p01 (accessed on October 2024).

[28] Ishiyama, Y. (2011). Introduction to Earthquake Engineering and Seismic Codes in the World. Lecture Note, Hokkaido University, Hokkaido, Japan.

[29] The Japan Society of Seismic Isolation (JSSI). (2024). Seismic isolation structures worldwide. The Japan Society of Seismic Isolation (JSSI), Tokyo, Japan.

[30] Pietra, D., Pampanin, S., Mayes, R. L., Wetzel, N. G., & Feng, D. (2015). Design of base-isolated buildings. Bulletin of the New Zealand Society for Earthquake Engineering, 48(2), 118–135. doi:10.5459/bnzsee.48.2.118-135.

[31] Wair, B. R., DeJong, J. T., & Shantz, T. (2012). Guidelines for estimation of shear wave velocity profiles. Pacific Earthquake Engineering Research Center, Berkeley, United States.

[32] JIS G 31122020. (2020). steel bars for concrete reinforcement. Japanese Standards Association (JIS), Tokyo, Japan.

[33] Bridgestone Corporation. (2024). Seismic isolation bearings for buildings. Bridgestone Corporation, Tokyo, Japan. Available online: https://www.bridgestone.com/products/diversified/antiseismic_rubber/ (accessed on October 2024).

[34] Oiles Corporation. (2024). Seismic isolator and vibration control devices. Oiles Corporation, Fujisawa, Japan. Available online: https://www.oiles.co.jp/en/products/damping_isolation/ (accessed on October 2024).

[35] Kawakin Corporation. (2024). Seismic isolation oil damper KYM. Kawakin Corporation, Kawaguchi, Japan. Available online: https://kawakinct.co.jp/en/product/#building (accessed on October 2024).

[36] AIJ. (2011). Simple calculation method for dynamic interaction between building and ground. Architectural Institute of Japan, Tokyo, Japan. (In Japanese).

[37] Shibata, A. (2010). Dynamic analysis of earthquake resistant structures. Tohoku University. Sendai, Japan.

[38] Saito, T. (2024). STERA WAVE technical manual version 1.0. Earthquake Disaster Engineering Research Laboratory, Toyohashi University of Technology, Toyohashi, Japan. Available online: https://rc.ace.tut.ac.jp/saito/software-e.html#p03 (accessed on October 2024).

[39] Takeda, T., Sozen, M. A., & Nielsen, N. N. (1970). Reinforced Concrete Response to Simulated Earthquakes. Journal of the Structural Division, 96(12), 2557–2573. doi:10.1061/jsdeag.0002765.

[40] Papanicolaou, G. C., & Zaoutsos, S. P. (2019). Viscoelastic constitutive modeling of creep and stress relaxation in polymers and polymer matrix composites. Creep and Fatigue in Polymer Matrix Composites, 3–59, Woodhead Publishing, Sawston, United Kingdom. doi:10.1016/b978-0-08-102601-4.00001-1.

[41] Jennings, P. C., & Bielak, J. (1973). Dynamics of building-soil interaction. Bulletin of the Seismological Society of America, 63(1), 9–48. doi:10.1785/bssa0630010009.

[42] Zhuang, H., Fu, J., Yu, X., Chen, S., & Cai, X. (2019). Earthquake responses of a base-isolated structure on a multi-layered soft soil foundation by using shaking table tests. Engineering Structures, 179, 79–91. doi:10.1016/j.engstruct.2018.10.060.

[43] Ismail, S. A., Kaddah, F. K., & Raphael, W. E. (2020). Effect of Number of Stories on the Seismic Soil Structure Interaction Performance of Midrise Frame Structures. IOP Conference Series: Materials Science and Engineering, 809(1), 012011. doi:10.1088/1757-899X/809/1/012011.